Eurographics Symposium on Rendering (2005)
Kavita Bala, Philip Dutré (Editors)

Inferring Reflectance Functions from Wavelet Noise

Pieter Peers Philip Dutré[†]

Department of Computer Science
Katholieke Universiteit Leuven

Abstract

This paper presents a novel method for acquiring a wavelet representation of the reflectance field of real objects. Key to our method is the use of wavelet noise illumination to infer a reflectance function for each pixel. Due to their stochastic nature, these wavelet noise patterns enable to trade off the number of recorded photographs for the quality of the computed reflectance functions. Additionally, each wavelet noise pattern affects all pixels in a recorded photograph, independently of the underlying material properties in the scene. Consequently, each recorded photograph contributes additional information to the reflectance field computation.

The presented method consists of three steps. First, a fixed number of photographs are recorded of the scene lit by a series of wavelet noise patterns emitted from a CRT monitor. Next, for each pixel a reflectance function is computed offline, by identifying the important wavelet coefficients for the pixel's reflectance function. The coefficients are computed by solving a linear least squares problem. Finally, once all reflectance functions are computed, a novel image of the scene can be composited with arbitrary incident illumination.

The method can be used for both image-based relighting and environment matting.

Categories and Subject Descriptors (according to ACM CCS): G.1.2 [Numerical Analysis]: Approximation; I.3.7 [Computer Graphics]: Three dimensional graphics and realism; I.4.1 [Image Processing and Computer Vision]: Digitization and Image Capture;

1. Introduction

To capture the appearance of real objects and to visualize them under novel illumination has received a lot of attention in recent years. A number of different methods have been developed. Most of these methods find their roots in *the Light Stage* [DHT*00] (i.e. Image-based relighting) or in *Environment matting* [ZWCS99]. Both techniques essentially try to solve the same problem, but use a radically different approach. Methods based on the Light Stage are traditionally better suited for scenes containing diffuse and slightly glossy materials, as opposed to Environment matting, which excels in capturing the reflections of highly glossy and specular objects. However, this disjunction has blurred with the introduction of newer techniques (e.g. [PD03, MLP04]).

A central concept in image-based relighting is a reflectance field; a $8D$ function expressing the relation between incident illumination at, and exitant illumination from an object for any position and direction. Capturing the complete $8D$ reflectance field requires an enormous amount of work. Therefore, image-based relighting techniques focus on capturing a dimensionally reduced ($4D$) slice of this function. The incident illumination is reduced to a $2D$ approximation by either restricting it to directional incident illumination, or by assuming it $2D$ positional parameterizable (i.e. directionally fixed). The exitant illumination is reduced to a $2D$ function by fixing the viewpoint. A reflectance function is defined as a $2D$ function by further fixing the view direction. It describes how a pixel in an image (recorded from the viewpoint) behaves under $2D$ incident illumination.

The goal of our method is to capture this $4D$ approximation of the reflectance field. Our method consists of three steps. In the first step a user-defined number of photographs of the scene are recorded. For each photograph the object is illuminated by a different wavelet noise pattern emitted from a CRT monitor. In the second step, a compact wavelet representation of the reflectance function is iteratively computed

[†] email: {pieterp, phil}@cs.kuleuven.ac.be

for each pixel separately. For each iteration, the most important wavelet is selected from a small set of candidates, and added to the reflectance function approximation. The candidate wavelets are inferred in a greedy manner from the already computed approximate reflectance function and their importance is estimated by solving a linear least squares problem. This process is repeated until all possible candidate wavelets are processed or a user-defined maximum is reached. Finally, in the third step, novel incident illumination or alternatively a backdrop image, can be applied to the computed reflectance functions, resulting in a relit image of the captured object.

The presented method has following properties:

- **Material types.** The method works equally well for diffuse, glossy and specular materials.
- **Mathematical framework.** A well defined mathematical framework forms the basis of our system (section 4).
- **The information gain is maximized per additional photograph.** In order to minimize the number of required illumination patterns and thus photographs, the information gain of each additional photograph should be maximized for computing the reflectance functions. Each emitted wavelet noise pattern affects all pixels in the recorded photographs, independently of the underlying material properties, resulting in additional information for the computation of each reflectance function.
- **Stochastic illumination patterns.** The illumination patterns (wavelet noise) are well defined, but contain a degree of randomness, enabling to trade off approximation accuracy versus the number of photographs. The user can choose to use less photographs at the cost of accuracy loss of the approximation of the reflectance functions.
- **The required dynamic range is minimized.** The average intensity of each illumination pattern is approximately equal by construction, therefore the same range of shutter times can be used for each photograph.
- **Compact representation.** To reduce storage cost, a compact non-linear wavelet representation of the reflectance field is used.
- **Simplicity.** The computation of the reflectance field, and of a relit image is simple and relatively fast.

2. Related Work

In this section we discuss work related to the acquisition of the reflectance field of real objects.

Sampling the reflectance field. Debevec et al. [DHT*00] created a gantry called the *Light Stage*, which samples the reflectance field by recording a series of photographs of an object from a fixed viewpoint. For each photograph, the object is illuminated from a single direction selected from a set of uniformly distributed lighting directions around the object. Subsequent versions improved on acquisition speed [HCD01], portability [MDA02, MGW01] and on reconstructing the reflectance functions more accurately [MPDW04]. The *Light Stage* has been successfully extended to include varying view points [MPN*02], animated human faces [HWT*04] and 4*D* incident lightfields [MPDW03].

Sampling the reflectance field using a Light Stage is suited for objects containing diffuse and directional diffuse materials, because their reflectance functions mainly contain low frequency components. The upper limit on the frequency components which can be captured is determined by the sampling rate (i.e. Nyquist rate). Capturing high frequency reflectance functions is impractical since the number of required samples scales linearly with the upper frequency limit.

Observing pixel responses under complex illumination. A number of techniques have been developed to overcome the problems of brute force sampling. Key to these methods is the use of a CRT monitor as "continuous" illumination device for emitting complex illumination onto the scene. A reflectance field is computed from the observed pixel responses of this complex illumination on the scene.

Environment matting, introduced by Zongker et al. [ZWCS99], uses horizontal and vertical two-color square wave patterns as input illumination. The response of a pixel is modeled by a box filter on the incident illumination. Chuang et al. [CZH*00] extended this idea by using multiple Gaussian filters instead of a single box filter. Oriented Gaussian strips are swept across the CRT screen and used as input illumination. Both methods require a non-linear optimization to find the parameters of the filters. The representational power of these filters is very limited, and only suited for objects containing specular, and, in the case of [CZH*00], highly glossy material properties. Wexler et al. [WFZ02] extended environment matting to a more general probabilistic model. [WFZ02] use natural images as input, but only demonstrate their system on specular objects.

Zhu and Yang [ZY04] model reflectance functions using a similar representation as [WFZ02]. Time varying cosine wave patterns, with a predetermined time frequency per pixel, are used as input. The main advantage of frequency based patterns is the robustness with respect to measurement noise. Using a different frequency per pixel would result in a large number of required illumination patterns. Therefore two series of patterns are used, each with a constant frequency for each row or column respectively. The method is biased towards elliptical Gaussian responses, due to the separation in horizontal and vertical patterns, and is therefore only suited for reflectance functions with a compact footprint, i.e. specular and glossy reflections.

Peers and Dutré [PD03] use wavelets as illumination patterns to selectively sample the reflectance field in the wavelet domain. A feedback loop is used to determine which part of domain is subsequently worthwhile to sample. Their method

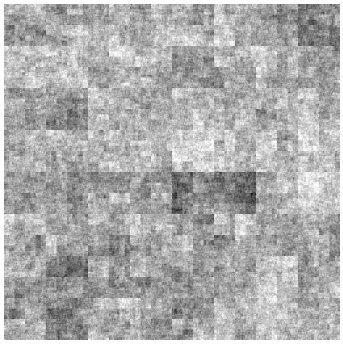

Figure 1: *An example of Haar wavelet noise.*

is able to capture the reflectance field of objects containing specular, glossy and diffuse material properties. The number of required photographs does not scale well for specular objects, since a small footprint wavelet illumination pattern contributes significantly to only a few pixels in the recorded photograph, resulting in a limited information gain from this photograph. Furthermore, the amount of light reflected from the object into the camera is closely related to the footprint size of the wavelet used in the illumination pattern, requiring a large dynamic range to accurately capture small and large footprint wavelet patterns.

Matusik et al. [MLP04] use natural illumination (i.e. photographs) as input. The reflectance function of each pixel is represented by a summation of weighted box filters, which are determined by a progressive algorithm. In each iteration of this progressive algorithm a constraint linear system is solved using Quadratic programming. A spacial correction is used to further enhance the results. [MLP04] demonstrate their technique on a number of objects containing specular, glossy and diffuse surfaces. It is not clear how many input images are required, or what the constraints are on the input illumination.

[MPZ*02] introduced a **hybrid method** that uses a Light Stage [DHT*00] to capture the low frequency part of the reflectance field, and an environment matting approach [CZH*00] to capture the high frequency part of the reflectance field.

3. Overview of the Method

Key to our technique is the use of wavelet noise illumination patterns. For each emitted wavelet noise pattern a high dynamic range photograph of the scene is recorded. Next, a progressive algorithm is used to compute a non-linear wavelet approximation of the reflectance function for each pixel.

A wavelet noise pattern is defined as the (monochromatic) wavelet composition of normal distributed random wavelet coefficients. An example of wavelet noise is shown in figure 1. Using wavelet noise as illumination patterns has a number of advantages:

- It is possible to generate any number of unique wavelet noise patterns. Together with the progressive computation of the reflectance functions, this enables to trade off between the number of illumination patterns and the quality of the final approximation.
- Because the wavelet noise patterns are globally defined in both time and frequency, each pixel gives a response, independent of the underlying reflectance function, when illuminated with a wavelet noise pattern. Thus, each additional photograph contributes new information for the computation of the reflectance functions.
- It is possible to fix the average of each wavelet noise pattern, resulting in a limited dynamic range which needs to be captured.

In this paper we describe the reflectance functions using a non-linear wavelet approximation. A progressive algorithm is used to infer the reflectance functions from the responses of the wavelet noise patterns for each pixel independently. The number of wavelet coefficients in the final approximation can be either user-defined or dynamically determined depending on the number of input illumination patterns. In order to progressively refine the approximation of the reflectance functions, a refinement oracle must be defined. A similar problem is addressed in [PD03] and in [MLP04]. Both use a progressive algorithm:

- In [PD03] a feedback loop is used to determine online which subsequent wavelet illumination patterns are important for the construction of the wavelet environment matte. The selection of these subsequent illumination patterns is based on information from already acquired photographs. The children of the wavelet, which resulted in the largest contribution to the wavelet environment matte (i.e. photograph with the largest L_2 norm), are selected to be processed in the subsequent iteration. Note that the selection of the wavelet illumination patterns is based on information gathered from all pixels in parallel, which can result in a non-optimal choice for individual pixels. Furthermore, it is possible that a child of another (less) important wavelet is more significant then the proposed wavelet illumination patterns.
- [MLP04] use a method in which box filters are split progressively based on the current approximation for each pixel independently. The splitting criterion, however, is not optimal as demonstrated in figure 2. Sub-figure 2.a shows an approximation (red) of a $1D$ representation of a reflectance function (blue). In sub-figure 2.b the approximation is refined by splitting the box filter with highest energy content (as is done in [MLP04]). However, in sub-figure 2.c a more optimal refinement, according to entropy, is shown.

In this paper a different refinement oracle, sharing compo-

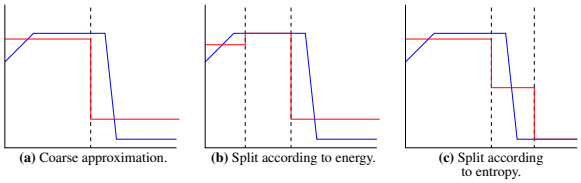

Figure 2: *(a) An approximation (red) of a 1D reflectance function (blue). (b) Refinement according to energy. A better refinement criterion in terms of error, would be according to entropy (c).*

nents from previous approaches, is used. In section 4.3, we will show that it is possible, for each pixel independently, to make an estimate of the magnitudes of the children's coefficients of the wavelets in the current approximation of the reflectance function. From these estimates, the wavelet with the largest coefficient is selected and added to the current approximation. The advantage of this approach is that the approximation is kept as small as possible, in terms of number of wavelet coefficients, while minimizing the approximation error.

In the next section (4) we develop a mathematical framework from which we will derive the algorithm described above.

4. Mathematical Framework

In this section a mathematical framework is developed for inferring reflectance functions from stochastically defined wavelet noise illumination. For an excellent introduction to wavelets and related mathematics we refer the reader to [SDS96]. First, the light transport is described for image-based relighting using a matrix notation (section 4.1). Using this notation, the properties of wavelet noise illumination are explored in section 4.2. Next, a progressive algorithm is developed to compute a reflectance function of a single pixel (section 4.3). Finally, in section 4.4 the normalization of the wavelet noise is discussed.

4.1. Light Transport Matrix

Light transport is a linear process which, for image-based relighting, can be written in a matrix notation:

$$C = \mathbf{T}\, L, \tag{1}$$

where L is the incident illumination, discretized in l parts, and stacked in a vector. C represents the resulting k pixel image, also stacked in a vector. The $l \times k$ matrix $\mathbf{T}$ represents the light transport. The goal of image-based relighting is to find $\mathbf{T}$ by controlling L and observing the resulting C.

Each row in $\mathbf{T} = [T_1, \ldots, T_k]$ represents a reflectance function of a single pixel in $C = [c_i]$, thus:

$$c_i = T_i \cdot L, \tag{2}$$

with T_i a vector of length l. Both L and $\mathbf{T}$ can be expressed in a basis $\mathbf{B}$ and corresponding dual basis $\overline{\mathbf{B}}$ [†]. $L_{\mathbf{B}}$, the projection of L on a basis $\mathbf{B}$, is defined as:

$$L_{\mathbf{B}} = \mathbf{B}\, L. \tag{3}$$

Define $\mathbf{T_B}$ the transport matrix expressed in the same basis $\mathbf{B}$:

$$\begin{aligned} C &= \mathbf{T}\, \overline{\mathbf{B}}\, \mathbf{B}\, L && (4)\\ &= \mathbf{T_B}\, L_{\mathbf{B}}. && (5) \end{aligned}$$

Note that the interpretation of the rows of $\mathbf{T_B}$ is similar as previously: the rows are the reflectance functions expressed in a basis $\mathbf{B}$.

4.2. Wavelet Noise Patterns

Define a wavelet noise pattern M_i as the sum of normal distributed random weighted wavelets:

$$M_i = \overline{\Psi}\, W_i, \tag{6}$$

where Ψ is a wavelet basis (with dual $\overline{\Psi}$) of l basis functions, and W_i is a vector of l normal distributed weights.

The observed camera image is (using formulas 1 and 3):

$$\begin{aligned} C &= \mathbf{T}\, M_i && (7)\\ &= \mathbf{T}\, (\overline{\Psi}\, \Psi)\, M_i && (8)\\ &= \mathbf{T}_{\Psi}\, \Psi\, M_i && (9)\\ &= \mathbf{T}_{\Psi}\, \Psi\, \overline{\Psi}\, W_i && (10)\\ &= \mathbf{T}_{\Psi}\, W_i. && (11) \end{aligned}$$

and thus the observed response c_p of a pixel p is:

$$c_p = T_{\Psi_p} \cdot W_i. \tag{12}$$

Denote $\mathbf{W} = [W_1 | \ldots | W_n]$, where each W_i is a column in $\mathbf{W}$, a set of wavelet noise patterns' weights. We would like to minimize n, the number of required illumination patterns,

[†] $\mathbf{B}\overline{\mathbf{B}} = \overline{\mathbf{B}}\mathbf{B} = \mathbf{I}$

and thus the number of photographs that need to be captured, such that $\mathbf{T}_\Psi$ can still be determined.

Since the reflectance function T_{Ψ_p} contains l entries, a brute force approach would require l wavelet noise patterns M_i and requires a linear system to be solved for T_{Ψ_p}:

$$C_p = T_{\Psi_p}\,\mathbf{W}, \tag{13}$$

where C_p is a vector containing the observed pixel values c_p for each W_i. However, Masselus et al. [MPDW04] noted that each T_{Ψ_p} can be compactly represented by a non-linear wavelet approximation. Suppose that each T_{Ψ_p} requires at most $m << l$ coefficients. If we know which m coefficients are significant, then an accurate estimate of the magnitude of these coefficients is possible using at least m wavelet noise patterns[‡] M_i. Denote $\widetilde{T_{\Psi_p}}^{(m)}$ the approximation of T_{Ψ_p} with m wavelet coefficients (i.e. zeroing out the least significant coefficients). Thus:

$$C_p \approx \widetilde{T_{\Psi_p}}^{(m)}\,\mathbf{W}. \tag{14}$$

If $\mathbf{W}$, C_p and the set of m significant coefficients, are known, then $\widetilde{T_{\Psi_p}}^{(m)}$ can be efficiently computed using a linear least squares minimization. Both $\mathbf{W}$ and C_p are known by either construction or acquisition. However, it is unknown which m coefficients are significant for a pixel p. Furthermore, each pixel p has a different set of m significant coefficients.

4.3. Progressive Refinement

In this section a progressive algorithm is developed to determine which subsequent wavelet coefficient is significant for a pixel p, given a set of m previously computed wavelet coefficients. First, we show that it is possible to use a progressive algorithm to infer the reflectance functions using the mathematical framework of the previous section. Next, a refinement criterion for progressively computing a reflectance function is derived.

A progressive algorithm is possible if a reliable estimate can be made of the magnitude of a subset of the significant wavelet coefficients. Therefore, reconsider equation 14 and extend it with an error term $E_p^{(i)}$:

$$C_p = (\widetilde{T_{\Psi_p}}^{(i)}\,\mathbf{W}) + E_p^{(i)}, \tag{15}$$

[‡] Generally, it is better to use more than m wavelet noise patterns, since it is possible that the m patterns are not completely orthogonal for the subspace spanned by the m non-zero wavelet coefficients.

Data: priorityQueue *processOrder*
list *waveletApproximation*

Init: add the scale function to *processOrder*

while(*maximum number of coefficients not reached* **and**
processOrder is not empty **and**
processOrder.top > *threshold*)
{
newWavelet = *processOrder.top*
add *newWavelet* to *waveletApproximation*
estimate the energy in each of the **direct children** which overlap the footprint of *newWavelet* (**Least Squares**)
insert children in *processOrder*
}
Re-estimate all selected wavelet coefficients (**Least Squares**) in *waveletApproximation* to arrive at the final solution.

Figure 3: *A high level description of the algorithm used to compute a reflectance function for each pixel.*

where $0 \leq i \leq m$. Combining with formula 13 we can write $E_p^{(i)}$ as:

$$\begin{aligned} E_p^{(i)} &= (T_{\Psi_p}\,\mathbf{W}) - (\widetilde{T_{\Psi_p}}^{(i)}\,\mathbf{W}) && (16)\\ &= (T_{\Psi_p} - \widetilde{T_{\Psi_p}}^{(i)})\,\mathbf{W} && (17)\\ &= R_p^{(i)}\,\mathbf{W}, && (18) \end{aligned}$$

where $R_p^{(i)}$ is the residue, containing the wavelet coefficients zeroed out in $\widetilde{T_{\Psi_p}}^{(i)}$. Note that $||R_{\Psi_p}^{(i)}||_2$ decreases as i increases. Furthermore $||R_{\Psi_p}^{(m)}||_2 \approx 0$.

The magnitudes of the entries in $E_p^{(i)}$ are distributed according to a normal distribution, since $\mathbf{W}$ follows a normal distribution by construction, and a weighted sum of normal distributions is a normal distribution itself. The mean of $E_p^{(i)}$ is zero, and the variance is determined by the magnitude of the elements in the residue $R_p^{(i)}$.

This implies that an estimate of the magnitude of the wavelet coefficients can be made, even if not all significant wavelet coefficients' positions are known, using a linear least squares minimization (formula 14). The error on the estimates decreases if the remaining most significant wavelet coefficients are added with increasing i. $\widetilde{T_{\Psi_p}}^{(i)}$ should contain the i largest coefficients, in order to minimize the error for each step. This shows that it is indeed possible to use a progressive algorithm using the framework set out in previous sections.

Given $\widetilde{T_{\Psi_p}}^{(i)}$, which wavelet coefficient should subsequently be added? We first note that if a wavelet has a

large response, then it is very likely that one or more of the children of this wavelet also have a significant response. This observation generally holds for natural functions such as reflectance functions. Furthermore, it is possible to estimate the coefficients of all the children of already computed wavelet coefficients in the current approximation. From these estimates, the child with largest entropy is selected and added to the current approximation. However, estimating all children at each iteration requires a significant overhead, not only in terms of computation, but also in terms of required number of illumination patterns. Estimating the coefficients of n children requires at least n additional illumination patterns. A solution to this dilemma is to only estimate the children of the wavelet that has been added most recently, and keeping the estimates of the children of previously added wavelets without re-evaluating them. The idea is that the relative error on large estimates is small, and thus the estimate will not change much in magnitude. However, the relative error on small estimates can be large, but this is not really a problem since we are mainly interested in large coefficients.

The resulting algorithm is shown in figure 3. There are three $2D$ wavelets associated with each position in space (i.e. $\psi_x\varphi_y$, $\varphi_x\psi_y$, $\psi_x\psi_y$, where ψ and φ are respectively the wavelet and the associated scale function). We store the total magnitude of all three wavelets as a single entry in the priority queue. When a specific wavelet position is retrieved from the queue, we estimate the direct children in the footprint of all three wavelets (i.e. 12 children for the Haar wavelet). Additionally, the priority queue is sorted according to intensity, and all three color channels are processed in parallel. The threshold in the algorithm in figure 3 ensures that we are not modeling camera noise.

4.4. Wavelet Normalization

In the previous sections we ignored the normalization of the wavelets in the illumination patterns. A number of wavelet normalizations are possible. When selecting a wavelet normalization, following factors need to be taken into account:

1. The wavelet noise patterns will be emitted from a CRT monitor (section 6). The number of distinct (linear) intensity values a CRT can generate is very limited (approximately 200). To allocate an equal intensity range to each individual wavelet, it is best that all wavelets have approximately the same amplitude. This way each wavelet occupies a $0.5log_2(l)$ part of the intensity range (worst case).
2. The algorithm described in figure 3 starts from the largest wavelet, and proceeds down to the children wavelets. This scheme works best if the wavelet coefficients do not gain in magnitude with advancing wavelet level. Using an equal amplitude across all wavelet levels ensures that small and large footprint wavelets are weighted equally.

There are two kinds of common wavelet normalizations:

Input: $\mathbf{Q^{(i-1)}}$, $\mathbf{R^{(i-1)}_{1:i-1}}$, $B^{(i-1)}$ and A_i
with $\mathbf{Q^{(0)}} = \mathbf{I}$, $\mathbf{R^{(0)}_{1:0}}$ = empty and $B^{(0)} = B$
Output: The solution to $\mathbf{A_{1:i}}X = B$

(1) $V_i = \mathbf{Q^{(i-1)^T}} A_i$
(2) compute the Householder reflection $\mathbf{H^{(i)}}$ using V_i
(3) $\mathbf{Q^{(i)}} = \mathbf{Q^{(i-1)}}\ \mathbf{H^{(i)}}$
(4) $\mathbf{R^{(i)}_{1:i}} = [\ \mathbf{R^{(i-1)}_{1:i-1}}\ |\ \mathbf{H^{(i)}}\ V_i\ ]$
(5) $B^{(i)} = \mathbf{H^{(i)}}\ B^{(i-1)}$
(6) back-substitute $\mathbf{R^{(i)}_{1:i}}X = B^{(i)}$ for X

Figure 4: *A sequential QR factorization algorithm for computing a least squares solution of* $\mathbf{A_{1:i}}X = B$ *for each iteration of the algorithm in figure 3.*

1. **Constant energy.** All wavelet have the same energy. (high-pass Nyquist gain = $\sqrt{2}$ and low-pass DC gain = $\sqrt{2}$).
2. **Constant amplitude.** All wavelets have approximately the same amplitude. (high-pass Nyquist gain = 2 and low-pass DC gain = 1).

Given the constraints, we opt for normalizing the wavelets in the wavelet noise patterns to a constant amplitude. The same normalization is used during computation of the reflectance functions. A disadvantage is that not necessarily the optimal non-linear wavelet approximation for a reflectance function in terms of energy conservation is computed.

5. Least Squares Minimization Speed Up

The algorithm in figure 3 requires a least squares minimization for each iteration during the computation of a reflectance function. A least squares minimization requires $O(m^2e)$ operations (e.g. using QR factorization), this is repeated m times. Thus the total operation count for the computation of a single reflectance function is $O(m^3e)$, where m is the number of coefficients to be computed, and e is the number of emitted patterns. However, this approach is not optimal, since a large number of operations is repeated between consecutive least squares minimizations. In figure 4 a sequential variant on the QR factorization algorithm is given for computing the reflectance function in $O(m^2e)$ time-complexity, instead of $O(m^3e)$. The algorithm is based on [DGKS76] (also in [Ste98] p339), and a mathematical derivation is given in appendix A. The most expensive step in the algorithm is (6), the back-substitution. To minimize the computational cost, the back-substitution should be postponed as much as possible, i.e. only back-substitute the elements that need to be estimated in the current iteration.

6. Data Acquisition and Calibration

Our acquisition setup consists of a CRT monitor and a digital camera (Canon EOS D30). Both the CRT monitor and the camera are radiometrically calibrated. The camera response curve is determined using the technique of [DM97], and each recorded photograph is converted to a high dynamic range image. A minimal shutter time of 1 second is used to avoid synchronization problems with the refresh rate of the CRT monitor. The gamma curve of the CRT monitor is measured by recording high dynamic range photographs of the CRT monitor while emitting 256 different intensity images. Since we only emit monochromatic wavelet noise patterns, no color calibration (except white balancing) is required. We did not fit an analytical gamma curve through the measured intensity values, but used the discrete representation directly. The discrete gamma curve is inversely applied before emitting a pattern.

There is a discrepancy possible between the intensity values used during computation and the intensity values actually emitted from the CRT monitor, since the discrete gamma curve can map multiple intensity values to the same screen value. To avert this, an inverse gamma correction followed by a forward gamma correction is applied to each pattern before computing a reflectance function.

7. Results and Discussion

To generate a relit image, the incident illumination is projected onto the wavelet basis. For each pixel a weighted sum of the wavelet coefficients from the reflectance function and the corresponding wavelet coefficients from the incident illumination is made, resulting in the relit pixel value.

In figures 6, 7 and 8 a number of results of our technique are shown. A reference photograph is shown, for each pair, on the left, while the computed relit image is depicted on the right. All examples are computed using 64 coefficients and 256 photographs. The resolution of the incident illumination is 512×512.

In figure 6, a hard disk is shown, illuminated from the right side by two different photographs. The scene contains specular (disk), glossy (cover) and diffuse (underground) material properties. The final computed reflectance field is 68MB LZW compressed (158MB uncompressed).

A detail of this scene, containing a balanced selection of different material properties, is used to test the influence of the number of coefficients versus the number of photographs. The results are depicted in figure 5. The red graph shows the error with respect to the reference image of a variable number of coefficients computed using 256 illumination patterns. A minimum was reached for 64 coefficients. Adding additional wavelet coefficients allows to approximate the reflectance function more accurately (e.g. from 32 to 64 coefficients), however, only a limited amount of information is available to estimate the coefficients, and thus, with each increase in the number of coefficients, the accuracy of the estimates decreases. At a certain point, the error on the estimates outweighs the addition in wavelet coefficients (e.g. from 64 to 96 coefficients). The green and blue graph show the error for respectively 64 and 128 coefficients when using a variable number of illumination patterns. As expected the error decreases with each additional illumination pattern.

The required processing time depends on the number of coefficients, the number of photographs, the underlying material property and the noise threshold. We tested a number of settings on the detail shown in figure 5. The timings for each setting ranged from 0.005 to 0.075 seconds per pixel on average, on a 3GHz Pentium 4 with 1GB of memory.

In figure 7 a scene is shown, inspired by [PD03]. Unlike previous methods, we also computed the reflectance functions of directly visible pixels on the CRT monitor. The final computed reflectance field is 139MB LZW compressed (329MB uncompressed).

Figure 8 shows an antique copper model replica of a Jaguar XK-120 illuminated from the right side by the two photographs used for figure 7. The final computed reflectance field is 58MB LZW compressed (132MB uncompressed).

All three results show some noise in dark areas. There are two sources of noise. Firstly, there is measurement noise, noticeable in regions with low reflectance. Secondly, there is some stochastic noise, due to the stochastic nature of the illumination patterns and estimation process (e.g. visible in figure 6, under the arch of the bridge). This stochastic noise shows some structure related to the (Haar) wavelet used. The amount of noise should decrease if the number of photographs increases.

The methods of [PD03] and [MLP04] are closest related to the presented method. What follows is a short comparison of the presented method and both previous methods. Both [MLP04] and our method have a straightforward data acquisition process, which is complicated in [PD03] by the feedback loop. The number of distinct wavelets in the computed reflectance functions were approximately 262000, which is almost equal to the total number of possible wavelets (given the resolution of the incident illumination). This gives an idea on how many wavelets have to be emitted to achieve similar results with the technique of [PD03]. [MLP04] solve a constraint linear least squares problem, which is more complex then solving an unconstraint linear least squares problem. Furthermore, [MLP04] requires a spacial correction to further enhance the results, which can fail if the scene contains many high frequency features. The presented method performed better when compared to the results of [MLP04] without spacial correction. We use a more optimal refinement criterion compared to both previous methods. Furthermore, it is unclear what the constraints are on the natural illumination used in [MLP04],

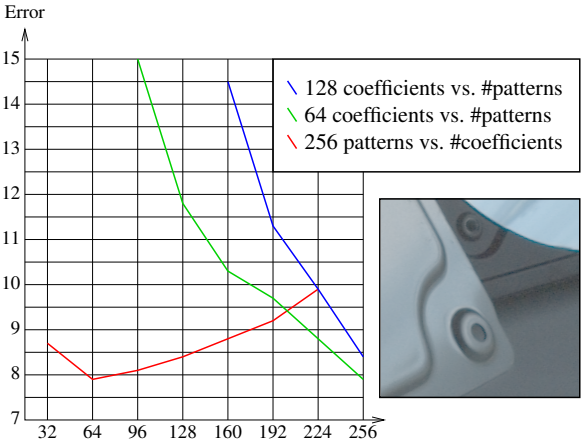

Figure 5: *The error on the approximation for the reference photograph in terms of the number of coefficients and the number of photographs. The error was computed on a detail of the scene from figure 6 and contains a balanced selection of diffuse, glossy and specular material properties. The red graph shows the error with respect to the number of coefficients when using* 256 *illumination patterns. The green and the blue graph shows the error on respectively* 64 *and* 128 *coefficients for a variable number of illumination patterns.*

whereas the wavelet noise patterns are well defined. A key difference, is that the wavelet noise patterns are dense in space and frequency, whereas this is not guaranteed for natural images.

8. Conclusions and Future Work

In this paper we presented a novel method for acquiring a compact wavelet representation of (a part of) the reflectance field of real objects. Wavelet noise patterns are used as input illumination and a progressive algorithm is used to compute the reflectance function for each pixel. The method works equally well for objects containing a mix of diffuse, glossy and specular materials. Using wavelet noise patterns has a number of advantages. Firstly, due to the stochastic nature of wavelet noise, any number of illumination patterns can be generated and used during measurement. This enables a trade-off between the accuracy of the approximation and the number of photographs which need to be recorded. Secondly, the information gain is maximized per additional photograph. The wavelet noise patterns are globally defined in space and frequency, resulting in a response on every pixel independent of the underlying reflectance function. Each additional photograph results in additional information for each pixel. Thirdly, the required dynamic range is minimized, because the wavelet noise patterns can be generated such that their average is approximately equal. The method is based on a solid mathematical framework and is easy to implement.

For future work we would like to investigate advanced filtering techniques directly on the wavelet representation of the reflectance field in order to reduce the stochastic noise in the computed results. Currently we are also looking into higher order wavelets. Initial experiments in this direction yield promising results. Furthermore, we would like to extend our method to use natural illumination as in [MLP04]. Natural illumination, however, does not result in normal distributed wavelet coefficients [DLAW01]. A thorough analysis on how far we can relax the constraints on the input illumination is required.

Acknowledgments

We would like to thank the anonymous reviewers for their constructive comments, and, Karl vom Berge, Ares Lagae and Saskia Mordijck for proof-reading. The first author is supported by K.U.Leuven grant GOA/2004/05.

References

[CZH*00] CHUANG Y.-Y., ZONGKER D. E., HINDORFF J., CURLESS B., SALESIN D. H., SZELISKI R.: Environment matting extensions: towards higher accuracy and real-time capture. In *SIGGRAPH '00: Proceedings of the 27th annual conference on Computer graphics and interactive techniques* (2000), ACM Press/Addison-Wesley Publishing Co., pp. 121–130. 2, 3

[DGKS76] DANIEL J., GRAGG W., KAUFMAN L., STEWART G. W.: Reorthogonalization and stable algorithms for updating the Gram-Schmidt QR factorization. *Math. Comp.* (October 1976), 772–795. ctr127. 6, 10

[DHT*00] DEBEVEC P., HAWKINS T., TCHOU C., DUIKER H.-P., SAROKIN W., SAGAR M.: Acquiring the reflectance field of a human face. In *SIGGRAPH '00: Proceedings of the 27th annual conference on Computer graphics and interactive techniques* (2000), ACM Press/Addison-Wesley Publishing Co., pp. 145–156. 1, 2, 3

[DLAW01] DROR R. O., LEUNG T. K., ADELSON E. H., WILLSKY A. S.: Statistics of real-world illumination. In *2001 IEEE Computer Society Conference on Computer Vision and Pattern Recognition (CVPR 2001), with CD-ROM, 8-14 December 2001, Kauai, HI, USA* (2001), IEEE Computer Society, pp. 164–171. 8

[DM97] DEBEVEC P. E., MALIK J.: Recovering high dynamic range radiance maps from photographs. In *SIGGRAPH '97: Proceedings of the 24th annual conference on Computer graphics and interactive techniques* (1997), ACM Press/Addison-Wesley Publishing Co., pp. 369–378. 7

[HCD01] HAWKINS T., COHEN J., DEBEVEC P.: A photometric approach to digitizing cultural artifacts. In *VAST*

'01: Proceedings of the 2001 conference on Virtual reality, archeology, and cultural heritage (2001), ACM Press, pp. 333–342. 2

[HWT*04] HAWKINS T., WENGER A., TCHOU C., GARDNER A., GÖRANSSON F., DEBEVEC P. E.: Animatable facial reflectance fields. In *Proceedings of the 15th Eurographics Workshop on Rendering Techniques, Norköping, Sweden, June 21-23, 2004 (Rendering Techniques '04)* (2004), Eurographics Association, pp. 309–321. 2

[MDA02] MASSELUS V., DUTRÉ P., ANRYS F.: The free-form light stage. In *EGRW '02: Proceedings of the 13th Eurographics workshop on Rendering* (2002), Eurographics Association, pp. 247–256. 2

[MGW01] MALZBENDER T., GELB D., WOLTERS H.: Polynomial texture maps. In *SIGGRAPH '01: Proceedings of the 28th annual conference on Computer graphics and interactive techniques* (2001), ACM Press, pp. 519–528. 2

[MLP04] MATUSIK W., LOPER M., PFISTER H.: Progressively-refined reflectance functions from natural illumination. In *Proceedings of the 15th Eurographics Workshop on Rendering Techniques, Norköping, Sweden, June 21-23, 2004 (Rendering Techniques '04)* (2004), Eurographics Association, pp. 299–308. 1, 3, 7, 8

[MPDW03] MASSELUS V., PEERS P., DUTRÉ P., WILLEMS Y. D.: Relighting with 4D incident light fields. *ACM Trans. Graph. 22*, 3 (2003), 613–620. 2

[MPDW04] MASSELUS V., PEERS P., DUTRÉ P., WILLEMS Y. D.: Smooth reconstruction and compact representation of reflectance functions for image-based relighting. In *Proceedings of the 15th Eurographics Workshop on Rendering Techniques, Norköping, Sweden, June 21-23, 2004 (Rendering Techniques '04)* (2004), Eurographics Association, pp. 287–298. 2, 5

[MPN*02] MATUSIK W., PFISTER H., NGAN A., BEARDSLEY P., ZIEGLER R., MCMILLAN L.: Image-based 3D photography using opacity hulls. *ACM Trans. Graph. 21*, 3 (2002), 427–437. 2

[MPZ*02] MATUSIK W., PFISTER H., ZIEGLER R., NGAN A., MCMILLAN L.: Acquisition and rendering of transparent and refractive objects. In *EGRW '02: Proceedings of the 13th Eurographics workshop on Rendering* (2002), Eurographics Association, pp. 267–278. 3

[PD03] PEERS P., DUTRÉ P.: Wavelet environment matting. In *EGRW '03: Proceedings of the 14th Eurographics workshop on Rendering* (2003), Eurographics Association, pp. 157–166. 1, 2, 3, 7, 11

[SDS96] STOLLNITZ E. J., DEROSE T. D., SALESIN D. H.: *Wavelets for computer graphics: theory and applications*. Morgan Kaufmann Publishers, Inc., 1996. 4

[Ste98] STEWART G. W.: *Matrix Algorithms: Volume 1: Basic Decompositions*. Society for Industrial and Applied Mathematics (SIAM), 1998. 6, 9, 10

[WFZ02] WEXLER Y., FITZGIBBON A. W., ZISSERMAN A.: Image-based environment matting. In *EGRW '02: Proceedings of the 13th Eurographics workshop on Rendering* (2002), Eurographics Association, pp. 279–290. 2

[ZWCS99] ZONGKER D. E., WERNER D. M., CURLESS B., SALESIN D. H.: Environment matting and compositing. In *SIGGRAPH '99: Proceedings of the 26th annual conference on Computer graphics and interactive techniques* (1999), ACM Press/Addison-Wesley Publishing Co., pp. 205–214. 1, 2

[ZY04] ZHU J., YANG Y.-H.: Frequency-based environment matting. In *12th Pacific Conference on Computer Graphics and Applications (PG 2004), 6-8 October 2004, Seoul, Korea* (2004), IEEE Computer Society, pp. 402–410. 2

Appendix A: QR Factorization

In this appendix we first review *QR* factorization and how it can be used to solve a least squares problem (among others described in [Ste98]). Next a derivation of the algorithm shown in figure 4 is given. To solve a linear least squares minimization we rewrite the system $\mathbf{A}\,X = B$ using the *QR* factorization of $\mathbf{A}$:

$$\mathbf{A}\,X = B \tag{19}$$
$$\mathbf{QR}\,X = B \tag{20}$$
$$\mathbf{R}\,X = \mathbf{Q}^T\,B, \tag{21}$$

where $\mathbf{R}$ is an upper-triangle matrix, and $\mathbf{Q}$ is an orthogonal matrix. The last equation 21 can be efficiently solved using back-substitution and gives the solution in a least squares sense.

The matrices $\mathbf{R}$ and $\mathbf{Q}$ are defined using Householder reflections:

$$\mathbf{R} = \mathbf{R^{(n)}} = \mathbf{H^{(n)}}...\mathbf{H^{(1)}}\,\mathbf{A} \tag{22}$$
$$\mathbf{Q} = \mathbf{Q^{(n)}} = \mathbf{H^{(1)}}...\mathbf{H^{(n)}}. \tag{23}$$

The Householder reflection $\mathbf{H^{(i)}}$ is defined as:

$$\mathbf{H^{(i)}} = \mathbf{I} - 2\,V_i^T\,V_i, \tag{24}$$

where V_i is the householder vector of the i-th column of $R^{(i-1)}$. Note that $\mathbf{H^{(i)}}$ and $\mathbf{Q^{(n)}}$ are never explicitly computed, since a multiplication with $\mathbf{H^{(i)}}$ can be done in $O(me)$ operations using formula 24 directly.

Appending a Row to the QR Factorization

For each iteration of the algorithm in figure 3 an additional vector A_i is determined and appended to $\mathbf{A}$. To minimize repeating computations through each iteration we first determine how $\mathbf{Q^{(i)}}$ and $\mathbf{R^{(i)}}$ change for each step.

The matrix $\mathbf{Q^{(i)}}$ is trivially dependent on $\mathbf{Q^{(i-1)}}$:

$$\mathbf{Q^{(i)}} = \mathbf{Q^{(i-1)}}\ \mathbf{H^{(i)}}. \tag{25}$$

The relation between $\mathbf{R^{(i)}}$ and $\mathbf{R^{(i-1)}}$ can be written as:

$$\begin{aligned} \mathbf{R^{(i)}} &= \mathbf{H^{(i)}} \ldots \mathbf{H^{(1)}}\ \mathbf{A} && (26)\\ &= \mathbf{H^{(i)}}\ \mathbf{Q^{(i-1)}}^T\ \mathbf{A} && (27)\\ &= \mathbf{H^{(i)}}\ \mathbf{R^{(i-1)}}. && (28) \end{aligned}$$

The problem is that $\mathbf{A}$ is not yet fully known. Define $\mathbf{A_{1:i}} = [A_1|\ldots|A_i]$, then:

$$\begin{aligned} \mathbf{R^{(i)}_{1:i}} &= \mathbf{H^{(i)}} \ldots \mathbf{H^{(1)}}\ \mathbf{A_{1:i}} && (29)\\ &= \mathbf{Q^{(i)}}^T\ [\mathbf{A_{1:i-1}} \mid A_i] && (30)\\ &= \mathbf{H^{(i)}}\ [\mathbf{Q^{(i-1)}}^T\ \mathbf{A_{1:i-1}} \mid \mathbf{Q^{(i-1)}}^T A_i] && (31)\\ &= \mathbf{H^{(i)}}\ [\mathbf{R^{(i-1)}_{1:i-1}} \mid \mathbf{Q^{(i-1)}}^T A_i] && (32)\\ &= \mathbf{H^{(i)}}\ [\mathbf{R^{(i-1)}_{1:i-1}} \mid V_i] && (33)\\ &= [\mathbf{R^{(i-1)}_{1:i-1}} \mid \mathbf{H^{(i)}}\ V_i]. && (34) \end{aligned}$$

This last step is possible since $\mathbf{H^{(i)}}$ does not effect columns 1 to $i-1$ (formula 24). Note that $\mathbf{R^{(n)}_{1:n}} = \mathbf{R^{(n)}}$. It is also immediately clear that the vector V_i, needed for creating the Householder reflection $\mathbf{H^{(i)}}$, is $\mathbf{Q^{(i-1)}}^{\mathbf{T}} A_i$.

Defining $B^{(i)} = \mathbf{Q^{(i)}}^{\mathbf{T}} B$, and using formula 34, 25 and 21, we can formulate the algorithm in figure 4. At each step of the algorithm the solution of $\mathbf{A_{1:i}}\ X = B$ is computed. The complexity of this algorithm is $O(me)$ for each iteration. The iteration is repeated m times, resulting in a total complexity of $O(m^2 e)$. The algorithm is due to [DGKS76] (also in [Ste98] p339).

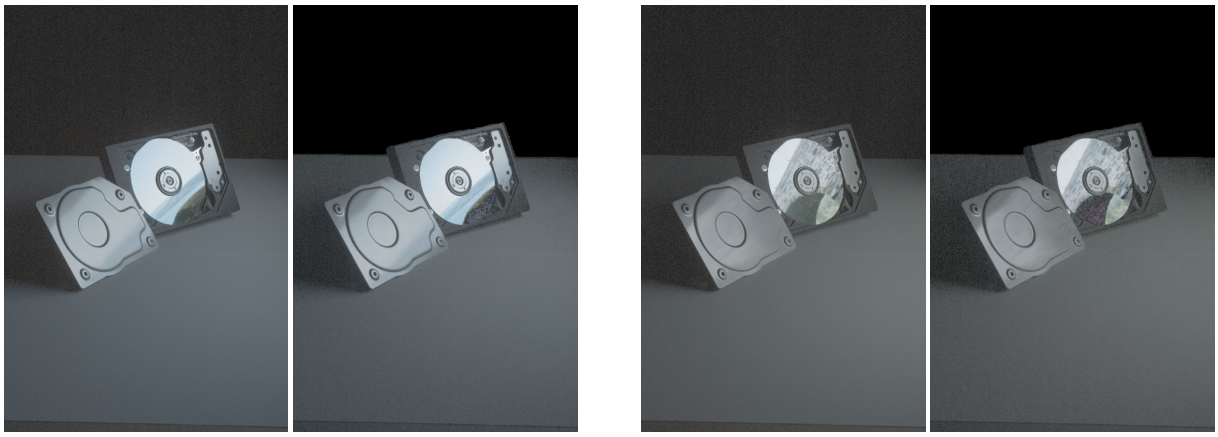

Figure 6: *A hard disk illuminated from the right side. The scene contains specular (disk), glossy (cover) and diffuse (underground) material properties. For each pair, a reference photograph is shown on the left, and a computed relit image on the right. The examples are illuminated by respectively a photograph of a landscape and a photograph of an old stone bridge.*

Figure 7: *A dinner scene, inspired by [PD03], illuminated from behind. Note that the directly visible pixels on the CRT are also computed using our method. For each pair a reference photograph is shown on the left.*

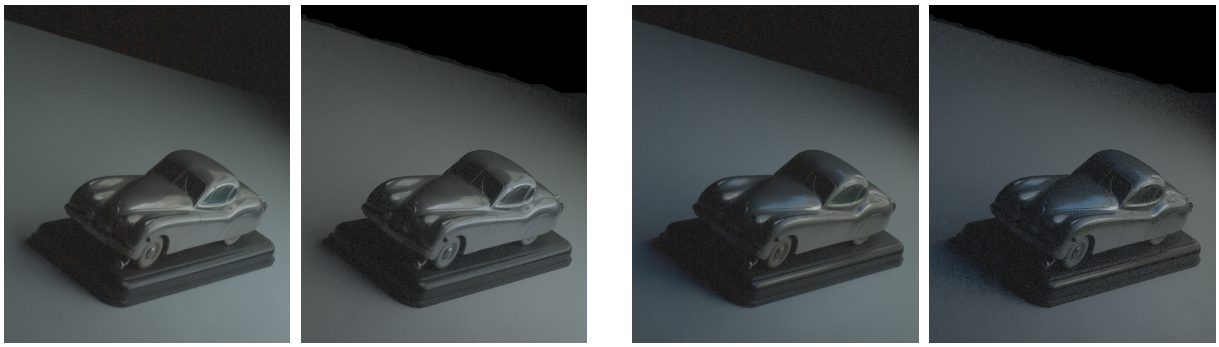

Figure 8: *An antique copper model replica of a Jaguar XK-120, illuminated from the right side. For each pair, a reference photograph is shown on the left. The scene is lit by the same photographs as in figure 7.*